HORIZONTAL TAIL LOCAL ANGLE-OF-ATTACK AND TOTAL PRESSURE MEASUREMENTS THROUGH STATIC PRESSURE PORTS AND KIEL PITOT

Rodrigo M. Granzoto*, Luiz A. Algodoal V.*, Gustavo J. Zambrano*, Gilberto G. Becker*
***Embraer S.A**

Keywords: *aerodynamics; CFD; flight-test; horizontal tail; angle-of-attack; sensor calibration*

Abstract

Aircraft handling qualities may be influenced by wing tip flow separations and horizontal tail reduced efficiency caused by loss of local dynamic pressure or local tailplane flow separations in high angle-of-attack maneuvers.
From the flight testers perspective provided the test aircraft presents sufficient longitudinal control authority to overcome an uncommanded nose up motion, this characteristics should be no safety factor.
Monitoring and measuring the local airflow in aircraft horizontal tail (HT) provides, information for safe flight test envelope expansion and data for early aerodynamic knowledge and model validation.
This work presents the development, installation, pre-flight calibration using computational fluid dynamics (CFD), flight test calibration, results and benefits of differential pressure based local angle-of-attack and total pressure measurements through 20 static pressure ports and a Kiel pitot.
These sensors were installed in a single-aisle, four-abreast, full fly-by-wire medium-range jet airliner with twin turbofan engines and conventional horizontal tail (low vertical position).

1 Introduction

As an important part of the preparation for the high incidence envelope expansion flight test campaign, the aircraft longitudinal stability and the possible tendency for uncommanded pitch movements must be considered. Newer aircraft models, with increased aspect ratio and swept wings, higher efficiency flaps, higher bypass engines (increased diameter) and, finally, lower horizontal tail area combined with more aft center-of-gravity positions, have led to a concern over achieving more critical stability and controls characteristics during stall maneuvers. Particularly, the aircraft handling qualities characteristics may be influenced by wing tip flow separations and horizontal tail reduced efficiency caused by loss of local dynamic pressure or local tailplane flow separations in high angle-of-attack maneuvers.

From the flight testers perspective, provided the test aircraft presents sufficient longitudinal control authority to overcome an eventual uncommanded nose up motion, this characteristics should be no safety factor.

Once the flight mechanics analysis of test airplane showed the longitudinal control authority to be safe enough to cope with all the test conditions, there will still be the need for real time monitoring during the test execution to assure the assumptions and the models used for all the previous analysis were valid.

Two key parameters have been successfully used in flight to accomplish this need for real time monitoring:

- Horizontal tail local angle-of-attack (α_{HT}); and
- Dynamic pressure measurements, particularly the ratio between the free stream dynamic pressure and the horizontal tail local dynamic pressure (η).

The first one (α_{HT}) copes with the risk of reaching a tailplane stall, which decreases aircraft longitudinal stability and may lead to an uncommanded pitch movement. The second one

(η) copes with a possible reduction in longitudinal stability and control authority of a non-stalled tail due to low dynamic pressure (i.e. due to engine or wing flow paths passing thought the tail position).

Monitoring and measuring the local airflow in aircraft horizontal tail (HT) provides, thus, information for safe flight test envelope expansion and data for early aerodynamic knowledge and model validation.

This work presents the development, installation, pre-flight calibration using computational fluid dynamics (CFD), flight test calibration, results and benefits of differential pressure based local angle-of-attack and total pressure measurements through 20 static pressure ports and a kiel pitot.

These sensors were installed in a single-aisle, four-abreast, full fly-by-wire medium-range jet airliner with twin turbofan engines and conventional horizontal tail (low vertical position).

2 Sensors Installation

Once identified the need for real-time monitoring of HT local angle-of-attack, several options of different sensors were considered. Most of the available sensors, such as angle-of-attack vanes, smart probes, etc would have similar calibration challenges, but would significantly affect the HT structural characteristics; in addition, most of already available sensors, due to its size and ideal locations were considered to interfere with the local airflow, thus interfering with the local α_{HT} measurement itself.

The search for a local angle-of-attack measurement that would not significantly affect the HT structural design and also be non airflow-interferant led to a differential static pressure solution. This solution only requires small pressure ports (small holes) adequately located to be sensible to small pressure differences between the upper and lower surfaces of the HT airfoil. Those differential pressure measures are physically correlated to local AOA variations.

The static pressure ports were designed to be located on the leading edge of HT. This location was chosen due to two different aspects:

1. Presents a higher sensitivity of static pressure coefficient (C_P) due to α_{HT} variation,
2. Easiness of installation and maintenance, once the pressure transducers can be installed with the removal of the horizontal tail leading edge, which is usually removable in most airplanes for several other reasons (for example anti-ice piccolo tubes installation).

As the differential pressure ports are susceptible to blockage and local disturbances and considering the safety effects of a wrong measure for real time monitoring during flight test, it was chosen a conservative, robust and redundant design: the differential pressure ports were distributed along ten chord positions for two distinct sections along the HT span. For this purpose, an averaging and a voting algorithm were employed for the final α_{HT} measurement.

Fig 1 shows the schematic architecture of the system.

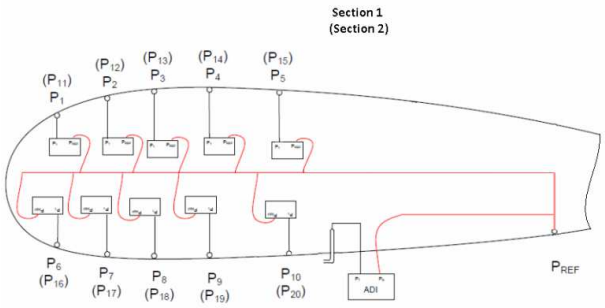

Fig 1 – Schematic system architecture of the system

Considering the needs for quick time response, good accuracy and resolution, the Honeywell PPT0002DNN2VB-S068 differential pressure sensor was chosen.

Honeywell PPT0002DNN2VB-S068 specifications[4]:
Digital Accuracy: ±0.05% FS

Analog Accuracy: ±0.06% FS
Operating Temperature: -40 to 85ºC
Storage Temperature: -55 to 90ºC
Sample Rate: 8.33ms to 51.2min
Digital Resolution: up to ±0.0011% FS
Analog Resolution: 1.22mV
Long Term Stability: 0.025% FS per year
Range: ±2 psi

Since the PPT0002DNN2VB-S068 needs to be connected to the reference pressure using capillary tubes, to avoid a possible pressure wave lag in the final measure, a single static pressure (P_{ref}) reference port was chosen and positioned as close as possible to transducers minimizing the tubes length and consequently its internal air volume. The P_{ref} was located in the lower side of HT.

The local dynamic pressure was measured through a kiel pitot installed on the lower side of the HT using a pre-existent access panel for easiness of installation and maintenance. The Kiel pitot vertical position was chose to keep it out of the boundary layer.
Fig 2 provides detailed information for the position of installed pressure ports, pressure transducers and kiel pitot.

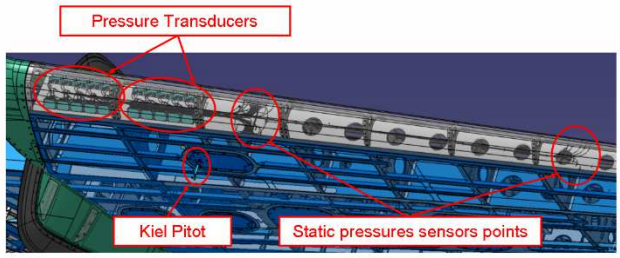

Fig 2 - HT sensors positions and installation

3 Pre-Flight Sensors Calibration

The non-interfering differential pressure solution adopted does not provide a direct local AOA measurement thus requiring means to convert differential pressure measurements in angle-of-attack measurements.

To develop the proper correlation between differential pressure and local angle-of-attack, an estimation of the α_{HT} (pre-flight) was done using CFD.

The local α_{HT} measure was assumed to be comprised of the following components:

1. Effects of pressure coefficient and elevator deflection on α_{HT} (α_{HT1}), since the local pressure and lift distributions are directly correlated with local angle of attack and elevator deflection.
2. Effect of aircraft free stream angle of attack (α) and flap angle (α_{HT2}), since the wing lift and downwash interferes with local HT airflow and changes the chordwise and spanwise distribution of local lift on HT.
3. Effect of HT incidence (α_{HT3}), since the relative geometric position of HT changes the aerodynamic interference characteristics between wing-tail and fuselage-tail, thus changing local HT pressure distribution.

In order to derive the relations to calculate α_{HT1}, α_{HT2} and α_{HT3}, CFD Simulations were performed with Metacomp Technologies CFD++ code[1], to simulate subsonic airflow conditions.

Three different types of CFD simulations were run:

- Wing-Body-Pylon-Nacelle tailless aircraft (WBPN);
- Body-Horizontal-Tail (BH) wingless aircraft, with different elevator deflections;
- Complete aircraft (WBPNH) with horizontal tail incidence variation.

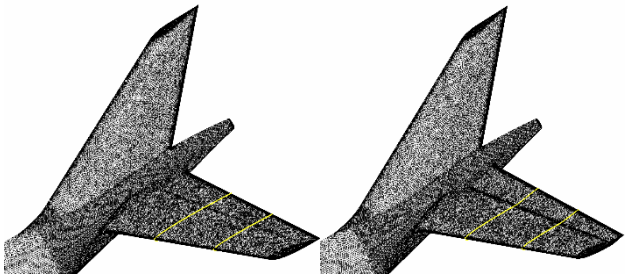

Fig 3 - Body-Horizontal-Tail mesh – with elevator two different elevator deflections

The grids are generated using the gridding guidelines based on EMBRAER experience. The flow is modeled using the Reynolds Averaged Navier-Stokes equations (RANS) with turbulence model closures. The time march is performed using a point-implicit method and using multigrid for convergence acceleration. In this work, the SA turbulence model is employed. The SA turbulence model is a well established closing model for aerospace industrial applications[2].

The Body-Horizontal-Tail (BH) CFD results were post-processed to provide α_{HT1}, i.e. the direct correlation between differential pressure and local angle of attack, for different elevator angles. For each pressure port location, a local angle-of-attack α_{HT1} was derived as function of C_P and elevator deflection. As these runs have no wing effect, the HT angle-of-attack is the same as free stream angle-of-attack. Fig 4 shows the correlation between C_P and α_{HT1} for the five pressure ports at upper side of HT in the section 1 with zero elevator deflection.

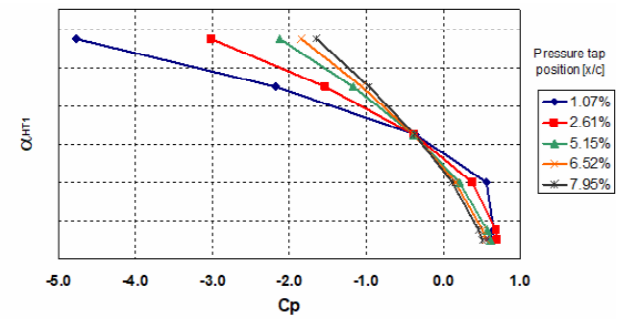

Fig 4 - Example of α_{HT1} as function of C_P for some pressure taps

The α_{HT2} was calculated using WBPN CFD runs with wing interference results calculated at 25% of local HT chord virtual position for each spanwise HT section, as it may be seen by Fig 5. Fig 6 shows the local alpha spanwise distribution as a function of free-stream α for the landing flaps configuration.

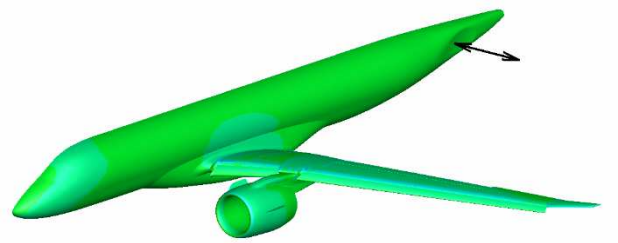

Fig 5 – Wing-Body-Pylon-Nacelle configuration CFD runs showing wing and engine effects on local virtual HT position

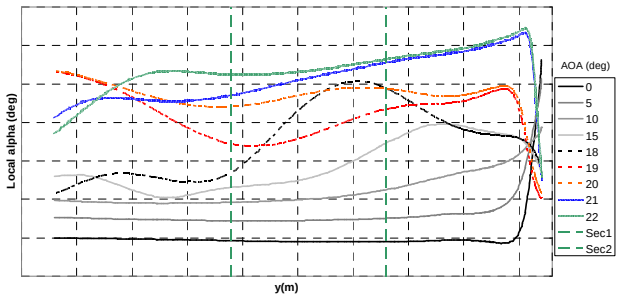

Fig 6 - Local angle of attack at virtual HT position as a function of span position for various aircraft angle-of-attack – landing flaps configuration

The α_{HT3} was calculated through CFD runs with WBPNH configuration with horizontal tail incidences of 0deg, -3deg and -6deg. thus providing corrections for the interference due to the local geometric incidence.

Equations (1) to (5) summarize the steps to calculate the final α_{HT} taking into account each sensor n of each section S.

Local α_{HT} for each section takes into consideration the mentioned the three effects (α_{HT1}, α_{HT2} and α_{HT3}) according to Equation (1).

$$\alpha_{HT_S} = \alpha_{HT1S} + \alpha_{HT2S} + \alpha_{HT3S} I_{HT} \qquad (1)$$

The α_{HT1} for each section *s* and for each pressure port *n* is a function of C_P and elevator

deflection. The final α_{HT1} is the mean of the values calculated for each of the ten sensors.

$$\alpha_{HT1S} = f(C_{Pn}, \delta_e) = \frac{1}{10} \times \sum_{n=1}^{10} \alpha_{HT1n} \qquad (2)$$

The α_{HT2} for each section is a function aircraft free-stream angle of attack and flap deflection angle.

$$\alpha_{HT2S} = f(\alpha, \delta_{flap}) \qquad (3)$$

The α_{HT3} for each section is an interference correction which is function of free-stream angle-of-attack, flap deflection angle, and horizontal tail incidence.

$$\alpha_{HT3S} = f(\alpha, \delta_{flap}, I_{HT}) \qquad (4)$$

The final value of α_{HT} is the mean of the calculated values for each of the two spanwise sections.

$$\alpha_{HT} = \frac{1}{2} \times \sum_{S=1}^{2} \alpha_{HTS} \qquad (5)$$

All 20 differential pressure transducers are connected to a reference static pressure port (P_{ref}). As a consequence, each transducer measures a differential pressure ΔP_n relative to the reference static port P_{ref}.

It is possible to convert the measure from the reference point to free-stream values by Equation (6), which uses free-stream static pressure (P_∞) and dynamic pressure (Q_∞). These quantities may be provided by airplane anemometric system or measured by dedicated flight-test instrumentation sensors such as a trailing cone and aircraft kiel pitot.

$$C_{P_n} = \frac{\Delta P_n + P_{ref} - P_\infty}{Q_\infty} \qquad (6)$$

Fig 7 compares α_{HT} components contribution during a stall maneuver. The plot shows that α_{HT1} is the most significant component when compared to α_{HT2} and α_{HT3} by one order of magnitude. That is because **α_{HT2} and α_{HT3}** are interference corrections factors and **α_{HT1}** is directly correlated to C_P.

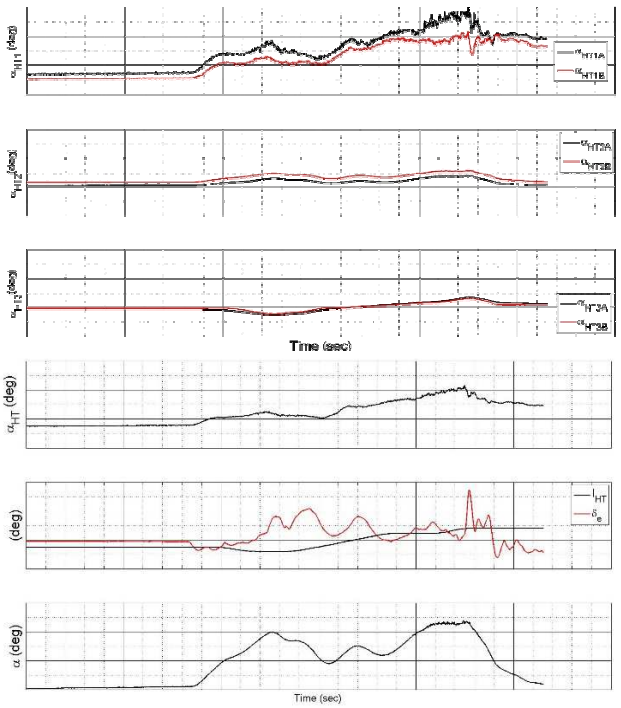

Fig 7 - α_{HT} components contribution comparison during a flight test stall maneuver

4 Flight Test Calibration

The flight test calibration of α_{HT} was based on the principle that when the aircraft angle-of-attack is kept constant, wing downwash may be assumed also constant. If it is possible to change horizontal tail incidence without changing aircraft angle of attack, the resultant change in HT incidence (ΔI_{HT}) should be equal to the change in local angle of attack ($\Delta\alpha_{HT}$).

The flight test procedure was based on the following steps:

- Trim the aircraft in a specified condition.
- Jam the elevator from the same side of sensors installation in a specified condition,

using a pre-defined function of flight-controls computer.

- Mistrim the aircraft using the trim switch and control the aircraft using the opposite side elevator to compensate for the mistrim. This elevator is not jammed and does not influence the pressure sensors because it is not located in the same side of the pressure sensors.
- Keep airspeed and aircraft angle-of-attack constant during maneuver.

For static conditions, local α_{HT} is a function of aircraft downwash and local tail incidence. Equations (7) and (8) describe, respectively, the conditions before and after the aircraft is mistrimmed.

$$\alpha_{HT1} = \alpha_1 - \varepsilon_1 + I_{HT1} \tag{7}$$

$$\alpha_{HT2} = \alpha_2 - \varepsilon_2 + I_{HT2} \tag{8}$$

The flight-test calibration maneuver is performed varying the I_{HT} and keeping the remaining parameters constant, thus:

$$\alpha_1 = \alpha_2 \tag{9}$$

$$\varepsilon_1 = \varepsilon_2 \tag{10}$$

Subtracting Equation (7) from Equation (8) results:

$$\alpha_{HT1} - \alpha_{HT2} = I_{HT1} - I_{HT2} \tag{11}$$

$$\Delta\alpha_{HT} = \Delta I_{HT} \tag{12}$$

The quantities ΔI_{HT} and $\Delta\alpha_{HT}$ may be calculated in relation to trimmed initial condition. In order to satisfy Equation (12), it is applied a calibration factor K_1 multiplying $\Delta\alpha_{HT}$:

$$\Delta I_{HT} = K_1 \times \Delta\alpha_{HT} \tag{13}$$

This process is repeated for each elevator position, thus providing corrections for the direct relationship between local angle-of-attack, elevator deflection and local C_P. This process is also repeated for different angle-of-attacks and flap deflections and, as a consequence, provides corrections to the interference between wing and horizontal tail.

A flight data comparison between ΔI_{HT} and $K_1 \times \Delta\alpha_{HT}$ is presented in Fig 8, Fig 9 and Fig 10. The good correlation shows that the calibration factor was sufficient to capture the effects of wing interference and local pressure distribution for different elevator deflections. It is important the calibration has a good physics modeling to increase the correlation between theoretical and flight test data.

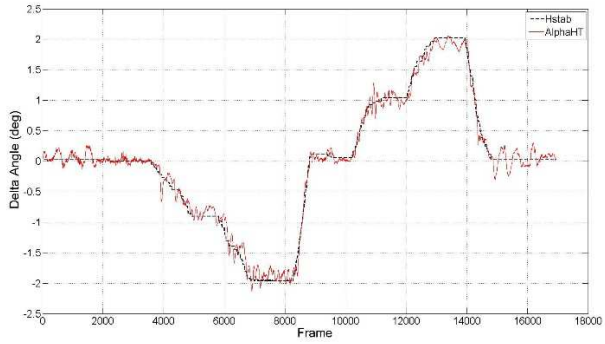

Fig 8 – Calibration flight test results – comparison between ΔI_{HT} and $K_1\Delta\alpha_{HT}$ – Cruise Flaps Configuration

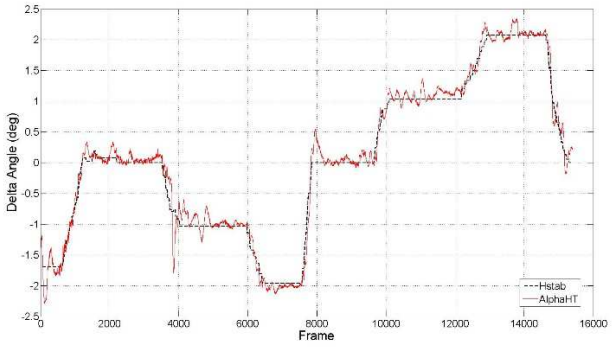

Fig 9 – Calibration flight test results – comparison between ΔI_{HT} and $K_1\Delta\alpha_{HT}$ – Take-off Flaps Configuration

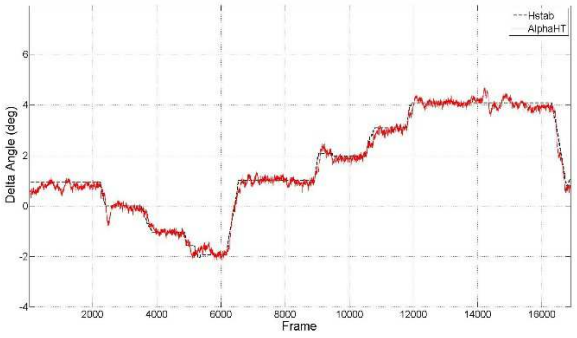

Fig 10 – Calibration flight test results – Comparison Between ΔI_{HT} and $K_1\Delta\alpha_{HT}$ – Landing Flaps Configuration

5 Flight-Test Results

The local HT angle-of-attack and dynamic pressure and the wing downwash are physically correlated to the aircraft inherent aerodynamic stability.

Understand how these variables compare to the predicted wind tunnel data is important in the early stages of aircraft flight-test development for safe envelope expansion and for aircraft control laws development and validation.

The differences between flight test and predicted wind-tunnel data may be used to improve existent flight-mechanics models. Data may be extrapolated for the more critical conditions, such as higher angle-of-attack and aft CG stall maneuvers. These new predicted data then may be compared with real time measurements of ε and α_{HT} during stall maneuvers, providing safe flight-test stop criteria if these parameters are out of a pre-determined range.

In aircraft with fly-by-wire systems, the control laws may be susceptible to aerodynamic model errors, particularly in the higher alpha region. The downwash and local-angle-of-attack measurements may be also used in conjunction with parameter-estimation techniques to improve linear models used by controls law gains updating. The early update of flight-controls laws is important to improve flight-test efficiency and to provide safer flight-test expansion.

During the stall maneuvers, the wing downwash (ε) may be computed for each time (t) step as a function of wing angle-of-attack (α), measured local angle-of-attack (α_{HT}) and horizontal tail incidence (I_{HT}). If the maneuver is not quasi-static, i.e. with high pitch and alpha rates, the downwash lag (τ) and the increase in local HT alpha due to the pitch rate (α_{HTdyn}) shall be considered:

$$\varepsilon(t-\tau) = \alpha(t) - \alpha_{HT}(t) + \alpha_{HTdyn}(t) + I_{HT}(t) \qquad (14)$$

Fig 11 shows such an example of computation that may be calculated real-time, during the execution of stall maneuvers. It shows a time-history comparison between flight test and predicted wind-tunnel simulation data for the parameters angle-of-attack, downwash, local HT angle-of-attack, horizontal tail incidence and elevator deflection.

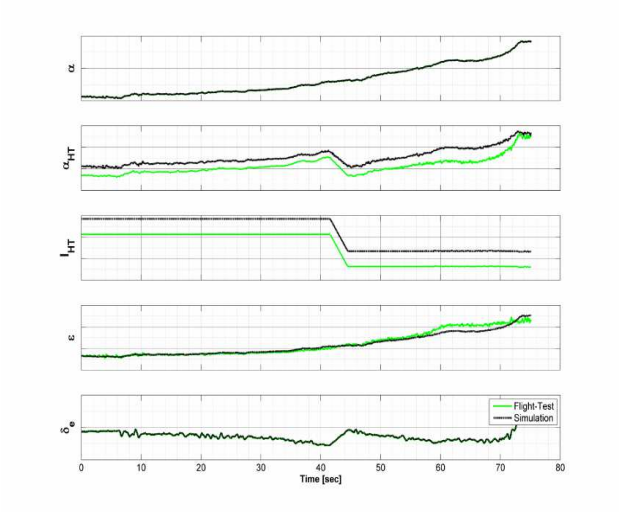

Fig 11 – α_{HT} and ε comparison between simulation predictions and flight-test data during a stall maneuver – Cruise Flaps Configuration

The measurement of horizontal tail characteristics was also combined with flow visualization techniques to provide information for validation and understanding of the aerodynamic characteristics of horizontal tail airflow. Fig 12 shows the flow visualization using tufts combined with measurements of HT angle-of-attack during a high incidence flight-test maneuver.

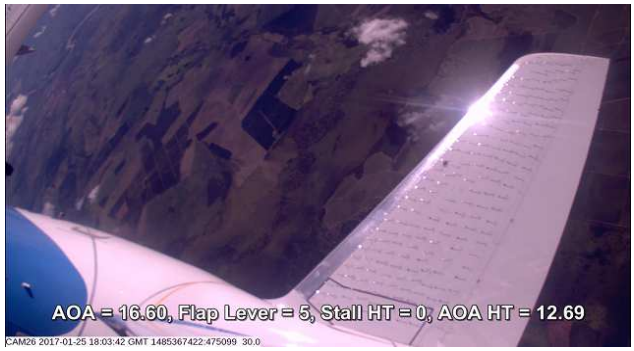

Fig 12 – Tufts flow visualization combined with HT measurements during a high incidence flight-test maneuver

Crossplots of wing downwash and aircraft angle-of-attack are shown in Fig 13 to Fig 16 for cruise, low take-off, high take-off and landing flaps configurations. The plots compare flight-test data (with and without calibration) with predicted wind-tunnel data.

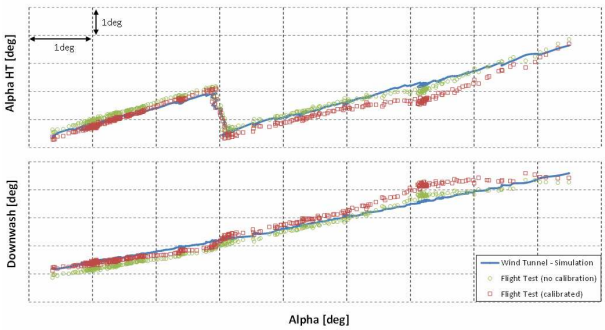

Fig 13 - Local α_{HT} and downwash comparison between wind-tunnel predictions and flight-test data during a stall maneuver – Cruise Flaps Configuration

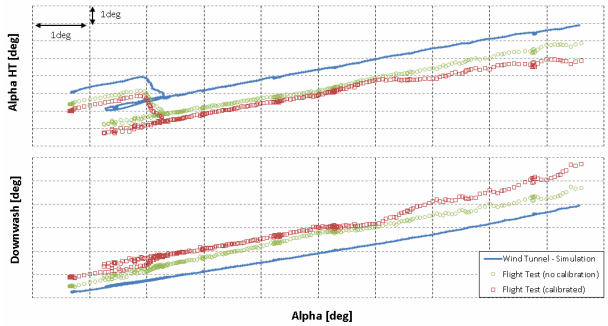

Fig 14 - Local α_{HT} and downwash comparison between wind-tunnel predictions and flight-test data during a stall maneuver – Low Take-off Flaps Configuration

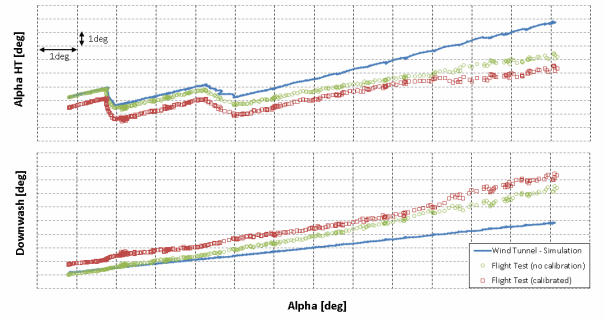

Fig 15 - Local α_{HT} and downwash comparison between wind-tunnel predictions **and flight-test** data during a stall maneuver – High Take-off Flaps Configuration

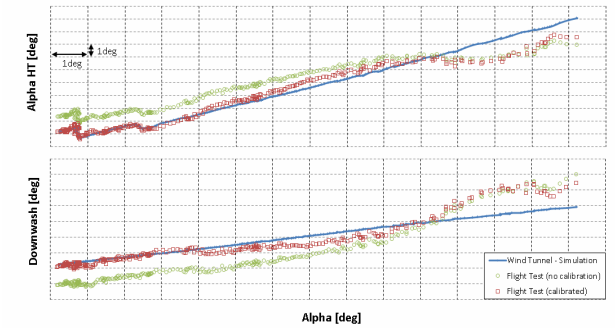

Fig 16 - Local α_{HT} and downwash comparison between wind-tunnel predictions and flight-test data during a stall maneuver – Landing Flaps Configuration

The results show that the differences between flight-test and predicted wind-tunnel data increase for higher angles-of-attack, probably due to higher interferences caused by wing and engine flow over the horizontal tail. These interferences may have different aerodynamic behavior between wind-tunnel and flight test (due to inherent wind-tunnel limitations such as geometric and Reynolds number differences) and also may affect the measurement and calibration of α_{HT} itself.

The dynamic pressure ratio as a function of aircraft angle-of-attack is shown in Fig 17 to Fig 20 for cruise, low take-off, high take-off and landing flaps configurations.

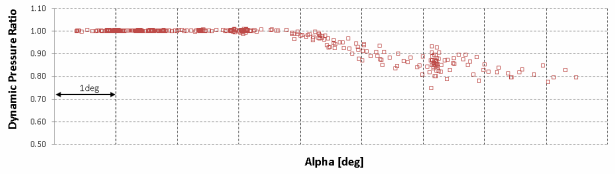

Fig 17 - Flight-test measurement of dynamic pressure ratio between local and global dynamic pressure (η) – Cruise Flaps Configuration

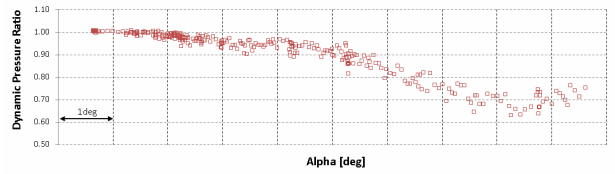

Fig 18 - Flight-test measurement of dynamic pressure ratio between local and global dynamic pressure – Low Take-off Flaps Configuration

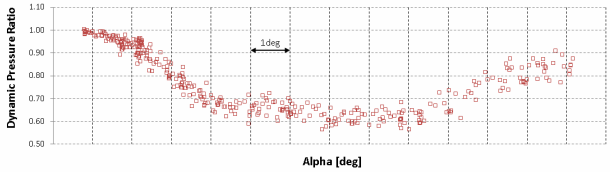

Fig 19 - Flight-test measurement of dynamic pressure ratio between local and global dynamic pressure (η) – High Take-off Flaps Configuration

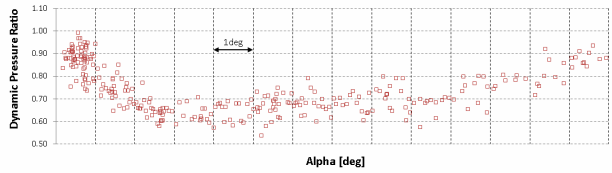

Fig 20 - Flight-test measurement of dynamic pressure ratio between local and global dynamic pressure (η) – Landing Flaps Configuration

The results show a significant loss of dynamic pressure at medium angles-of-attack, which decreases aircraft longitudinal stability and elevator efficiency. However, in the more deflected flaps configurations, which are the critical conditions for stall characteristics, the local dynamic pressure starts to increase again near the stall angle-of-attack, improving stability and control characteristics.

If such curves of Fig 13 to Fig 16 are linearized in the linear region of each curve, the wing downwash (ε) may be written as a function of downwash for zero angle-of-attack (ε_0) and a downwash slope ($d\varepsilon/d\alpha$), as in Equation (15).

$$\varepsilon = \varepsilon_0 + {d\varepsilon}/{d\alpha} \qquad (15)$$

Table 1 compares the linearized downwash parameters between flight-test and wind-tunnel data.

Table 1 – Differences between flight test results and estimated wind-tunnel parameters ε_0 and $d\varepsilon/d\alpha$

Configuration	**Error on ε_0**	**Error on $d\varepsilon/d\alpha$**
Cruise Configuration	0.4 deg	12.0%
Low Take-off Configuration	-0.6 deg	8.5%
High Take-off Configuration	0.2 deg	30.7%
Landing Configuration	-0.2 deg	18.8%

In general, the differences between flight-test and predicted wind-tunnel data (both in the linear and non-linear region) have shown that the expected maximum α_{HT} that would be achieved in the most critical maneuvers would always be less than the simulations model predicted, providing a safety margin for envelope expansion.

6 Conclusions

The choice of differential pressure based local HT AOA measurement showed the following advantages:

- Easiness of installation;
- No interference in the local airflow;
- Good correlation with theoretical data;
- Safe monitoring of an entire high angle-of-attack flight test campaign;
- Easiness of in-flight calibration procedure;
- Robustness to sensor port blockage (redundancy);
- Aerodynamics characteristics of flight-test airplane in conformity with production airplane.

The disadvantages observed during the use and operation of this sensor was:

- Sensitiveness to high moisture environment;

- Non suitability for use in the artificial ice shapes tests (due to installation of simulated ice shapes in the leading edge of the test aircraft HT).

References

[1] CFD++ Documentation", Metacomp Technologies Inc., retrieved from http://www.metacomptech.com, accessed in March, 2017.

[2] Leonardo C. Scalabrin, Pedro Ciloni, Alexandre Antunes, Gilberto G. Becker, Maximiliano A. Souza, and Rodrigo M. Granzoto. "EMBRAER Contribution to HiLiftPW-3", 2018 AIAA Aerospace Sciences Meeting, AIAA SciTech Forum, (AIAA 2018-1036).

[3] Joseph C. Eppel, Dennis W. Riddle, and Victor C. Steves" Flight Measured Downwash of the QSRA" Ames Research Center, Moffett Field, California 1988.

[4] Honeywell Precision Pressure Transducer (PPT) Data Sheet.

Contact Author Email Address

Rodrigo Milare Granzoto
Embraer S.A.
São José dos Campos - Brazil
Email: rodrigo.granzoto@embraer.com.br

Copyright Statement